nature communications

Article

https://doi.org/10.1038/s41467-025-58131-8

Structural insights into thyroid hormone transporter MCT8

Received: 28 June 2024

Accepted: 11 March 2025

Published online: 26 March 2025

Check for updates

Jiaxin Tan[1,2], Yuan Xiao[1,2], Fang Kong[1,2], Jiawei Qian[1], Angqi Zhu[1] & Chuangye Yan[1]

Thyroid hormones (THs), including T4 (3,5,3′,5′-tetraiodo-L-thyronine) and T3 (3,5,3′-triiodo-L-thyronine), play critical roles in regulating tissue development and basal metabolism. Monocarboxylate transporter 8 (MCT8) is a key player in TH transport, known for its high specificity and affinity for THs and its direct association with Allan-Herndon-Dudley syndrome (AHDS) caused by pathogenic mutations. In this study, we present the cryo-EM structures of human MCT8 bound to the substrate T3 or the inhibitor silychristin, both in an outward-open conformation at resolutions of 3.0-3.2 Å. MCT8 forms a homodimer with a lipid molecule positioned at the dimerization interface. The carboxyl group of T3 is recognized by Arg371, while its three iodine atoms interact with distinct hydrophobic cavities. Silychristin is also recognized by Arg371, competing with T3 for binding. Complemented by structure-guided biochemical analyses, our research elucidates the mechanisms of substrate recognition and transport, as well as the mode of action of the inhibitor silychristin. These findings may offer insights for developing targeted therapies for TH-related disorders.

Thyroid hormones (THs), including T4 (3,5,3′,5′-tetraiodo-L-thyronine) and T3 (3,5,3′-triiodo-L-thyronine), are iodinated amino acids produced by the thyroid gland. These hormones are widely recognized for their pivotal role in the development of virtually all tissues and the lifelong regulation of basal metabolism[1,2]. Several transporters facilitate the transport of THs across cell membranes, including the monocarboxylate transporters (MCTs) 8 and 10, organic anion transporter (OATP) 1C1, large neutral amino acid transporters (LATs) 1 and 2, and the sodium/taurocholate cotransporting polypeptide (NTCP)[3]. Among these, MCT8 is distinguished as the most specific and high-affinity transporter for THs, showing particular selectivity for these hormones over other aromatic amino acids[4,5].

The MCT family comprises 14 members, designated MCT1 to MCT14, which are responsible for transporting various monocarboxylates such as pyruvate, lactate, ketone bodies, carnitine, and aromatic amino acids[6]. Among these, MCT1-4 have been extensively studied for their roles in maintaining energy equilibrium and pH homeostasis through the proton-coupled transport of L-lactate, pyruvate, and ketone bodies. MCT8 has also emerged as one of the most studied MCT isoforms, functioning as a sodium- and proton-independent TH transporter[7]. MCT10 serves as an aromatic amino acid transporter and shares overlapping substrates with MCT8[8]. Recent structural advances in MCT1[9] and MCT2[10] have unveiled the molecular basis for recognizing small monocarboxylates. Given the high sequence homology between MCT1, MCT2, MCT8, and MCT10 (Supplementary Fig. 1), it is likely that similar mechanisms govern substrate recognition across these isoforms.

MCT8, encoded by the *SLC16A2* gene located on chromosome Xq13.2, is the only TH transporter with known pathogenic mutations in humans. Pathogenic variants of MCT8 are specifically linked to MCT8 deficiency or Allan–Herndon–Dudley syndrome (AHDS)[11,12], a rare genetic disorder characterized by intellectual disability and impaired motor control. Interestingly, MCT8 deficiency in mice does not result in severe neurological impairment[13]. This disparity is attributed to the

[1]Beijing Frontier Research Center for Biological Structure, State Key Laboratory of Membrane Biology, Tsinghua-Peking Joint Center for Life Sciences, School of Life Sciences, Tsinghua University, 100084 Beijing, China. [2]These authors contributed equally: Jiaxin Tan, Yuan Xiao, Fang Kong.
e-mail: yancy2019@tsinghua.edu.cn

compensatory expression of the transporter OATP1C at the blood-brain barrier (BBB) in mice—a mechanism absent in humans[14,15]. Reduced expression level of OATP1C1 in the human BBB underlies AHDS pathogenesis[16]. Despite ongoing efforts since the initial recognition of MCT8 deficiency, many pathophysiological aspects remain unclear, and therapeutic options are limited.

Thyroid follicular cells primarily secrete T4, but T3 is recognized as the biologically active TH responsible for most of its actions by binding to nuclear receptors[2,17,18]. The conversion of T4 to T3, along with their inactive metabolites such as rT3 (reverse T3, 3,3′,5′-triiodo-L-thyronine) and T2 (3,3′-diiodo-L-thyronine), is carried out through a deiodination process mediated by iodothyronine deiodinases (DIOs) 1–3[19,20]. MCT8 exhibits a ligand preference order of T3 > T4 > rT3 ≈ T2[21], highlighting its selectivity for the more active form of THs. High-resolution structural knowledge of MCT8 in complex with THs is important for understanding its transport mechanism and substrate specificity. Besides, MCT8 has been reported to exist as homodimers[22], but the dimerization mechanism are not yet fully understood.

To date, only a few drugs and natural compounds have been shown to interfere with MCT8 function. One such compound is silychristin, a flavonoid abundant in milk thistle fruits, known for its antioxidant and anti-inflammatory effects, particularly in conditions like hepatitis C infection and chronic liver disease[23]. Silychristin inhibits MCT8-mediated TH uptake, with an IC_{50} of 110 nM[24]. Despite its therapeutic use in liver disease, concerns have been raised about silychristin's potential adverse effects on the TH axis. Therefore, further structural insights are necessary to fully understand the mechanism by which silychristin inhibits MCT8 and to assess its potential implications for therapies targeting MCT deficiency.

In this study, we present two cryo-EM structures of wild-type (WT) human MCT8, each bound to substrate T3 and the inhibitor silychristin in an outward-open conformation, at resolutions of 3.0–3.2 Å. These high-resolution structures, together with our biochemical assays, offer detailed insights into the transport and inhibition mechanisms of MCT8.

Results

Structure determination of MCT8

The MCT8 construct, fused with a C-terminal FLAG tag, was transiently expressed in HEK293F cells. It was then purified using anti-FLAG affinity resin and subjected to size exclusion chromatography (SEC) on a Superose 6 column pre-equilibrated with 0.02% (w/v) glyco-diosgenin (GDN) (Supplementary Fig. 2a, b).

The GDN-purified MCT8 was analyzed using cryo-EM (Supplementary Fig. 2c, d). During cryo-EM sample preparation, the proteins were supplemented with either the substrate T3 at a final concentration of 1.5 mM or the inhibitor silychristin at a final concentration of 4 mM. After multiple rounds of 3D classifications and non-uniform refinements using cryoSPARC[25], we improved the resolutions of MCT8 in complex with substrate or inhibitor to about 3 Å (Supplementary Fig. 3). Both resulting structures exhibit a homo-dimeric state in an outward-open conformation. The density maps are of good quality with well-defined transmembrane domains (TMDs), enabling the clear identification of the bound substrate T3 or inhibitor silychristin (Fig. 1, Supplementary Fig. 4, 5 & Supplementary Table 1). Further details on sample preparation and data processing are provided in "Methods" section.

The dimerization interface

MCT8 adopts a typical Major Facilitator Superfamily (MFS)fold, with its 12 TMs organized into two six-helix bundle domains: the N-terminal domain (NTD, TM1-6) and the C-terminal domain (CTD, TM7-12). Purified MCT8 predominantly exists as a homodimer, with the two NTDs playing a key role in dimerization (Fig. 1a). This differs from MCT2, where dimerization involves both the NTD and CTD[10].

The dimerization interface of MCT8 is formed primarily by TM3 and TM6. Interestingly, a lipid molecule is anchored at this interface (Fig. 2a, b), a feature also observed in other membrane proteins such as the multiple peptide resistance factor MprF[26]. The lipid showcases a horseback-riding conformation at the interface (Fig. 2b). Specifically, the phosphate group of the lipid engages in hydrophilic interactions with Arg171 in each monomer, forming two hydrogen bonds. Meanwhile, the two hydrophobic tails of the lipid are situated within two lateral hydrophobic clefts, where they are accommodated by Ile172 and Leu278 from each monomer (Fig. 2c, left panel).

Residues from each monomer also contribute to dimerization through both hydrophobic and hydrophilic interactions. Specifically, the benzene rings of Phe182 and Phe271 from both protomers intersect to form two pairs of π-π interactions. In close proximity, Ala179, Met274, and Leu275 further enhance this hydrophobic interaction

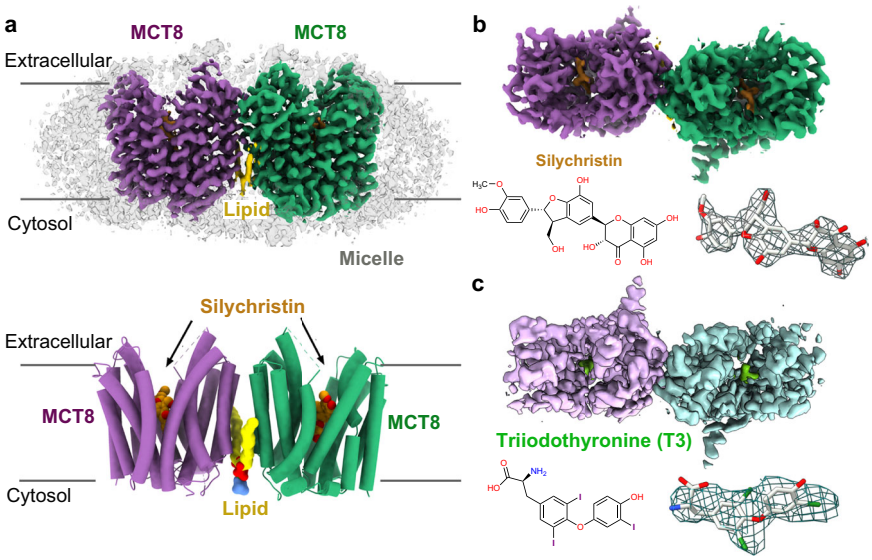

Fig. 1 | Overall structure of ligand-bound MCT8 homodimer. a Cryo-EM map and overall structure of MCT8. The two protomers of MCT8 are distinctly colored in violet and green, while lipids are depicted in yellow. MCT8 bound to silychristin was used. **b** Structure of MCT8 bound to silychristin. Silychristin is highlighted in brown in the cryo-EM map, with its chemical structure and density shown in the panel below. **c** Structure of MCT8 bound to triiodothyronine (T3). T3 is highlighted in green. The chemical structure and density of T3 are shown in the panel below. All density and structure figures were prepared using ChimeraX.

https://doi.org/10.1038/s41467-025-58131-8

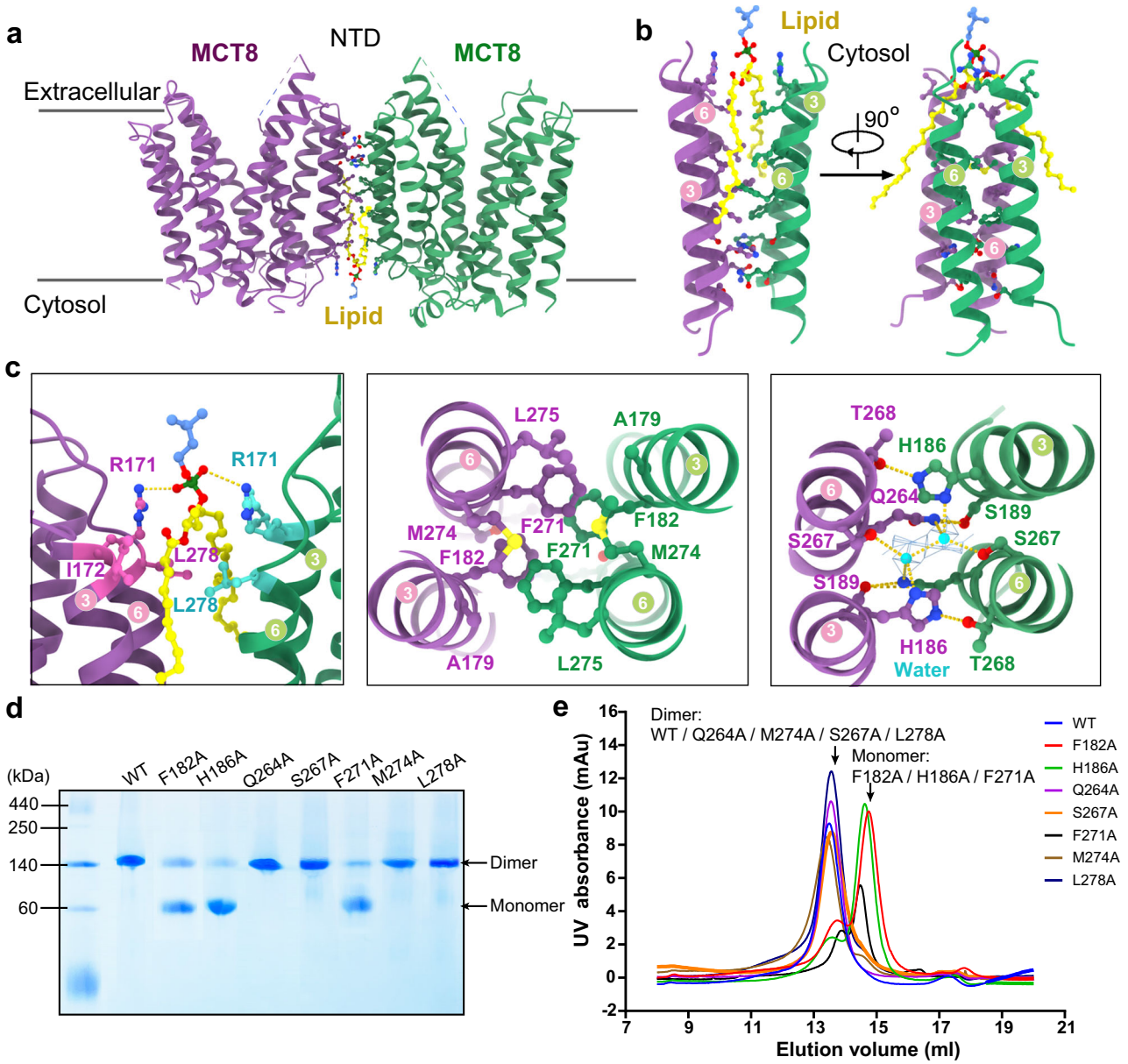

Fig. 2 | The MCT8 dimerization interface. a MCT8 homodimer stabilized by a lipid molecule. **b** Two perpendicular views of the MCT8 dimer interface, oriented with the cytosolic side up for illustration. **c** Three interacting clusters of MCT8 at the dimer interface. *Left panel:* a lipid molecule on the intracellular side interacts with Arg171 and surrounding hydrophobic residues. *Middle panel:* Phe182 and Phe271 from each monomer form two pairs of π-π interactions. Ala179, Met274 and Leu275 further stabilize this hydrophobic interactions. *Right panel:* Direct hydrogen bonds and water-mediated interactions are involved. The yellow dashed lines indicate hydrogen bonds. The blue spheres represents the water molecules. These water molecules are observed in the structure of MCT8 bound to silychristin. **d** The effect of dimer interface mutations on MCT8 dimerization. Dimer formation was assessed by blue native-PAGE analysis. WT MCT8 and the variants Q264A, S267A, M274A, and L278A primarily exist as dimers, whereas the variants F182A, H186A, and F271A predominantly exist as monomers. This experiment was independently repeated three times with similar results. **e** SEC analysis of MCT8 WT and variants. SEC results indicate the dimerization state of human MCT8 WT and mutations in the presence of 0.02% (w/v) GDN. Transfection quantity and expression cell volume were kept consistent for each mutant.

(Fig. 2c, middle panel). Hydrophilic interactions at the dimer interface are mediated by His186, which forms a water-mediated hydrogen bond with Ser267 and a direct hydrogen bond with Thr268 in the other protomer. Additionally, Gln264 establishes hydrogen bonds with the water molecule and Ser189, reinforcing the hydrophilic interactions (Fig. 2c, right panel). Due to the resolution limitations, these water molecules are only observed in the MCT8-silychristin structure. These interface residues are conserved across animals, with the exception of His186 and Thr268, which exhibit a coevolutionary pattern and are found exclusively in mammalian MCT8 (Supplementary Fig. 6a).

We further explored the function of these residues involved in MCT8 dimerization and their impact on substrate transport. Mutations of Phe182, His186, or Phe271 to Ala effectively disrupt MCT8 dimerization, as confirmed by blue native PAGE and gel filtration assays (Fig. 2d, e). These results align with our structural analysis. Interestingly, compared to the WT and other mutations at the dimerization interface that do not impair dimerization, these three mutations showed essentially no change in T3 uptake (Supplementary Fig. 6b). This suggests that preventing homodimer formation does not necessarily compromise in vitro TH transport.

T3 binds in central substrate site

The structure of MCT8 bound to its substrate T3 was solved in an outward-open state at a resolution of 3.13 Å. T3 is located within the

https://doi.org/10.1038/s41467-025-58131-8

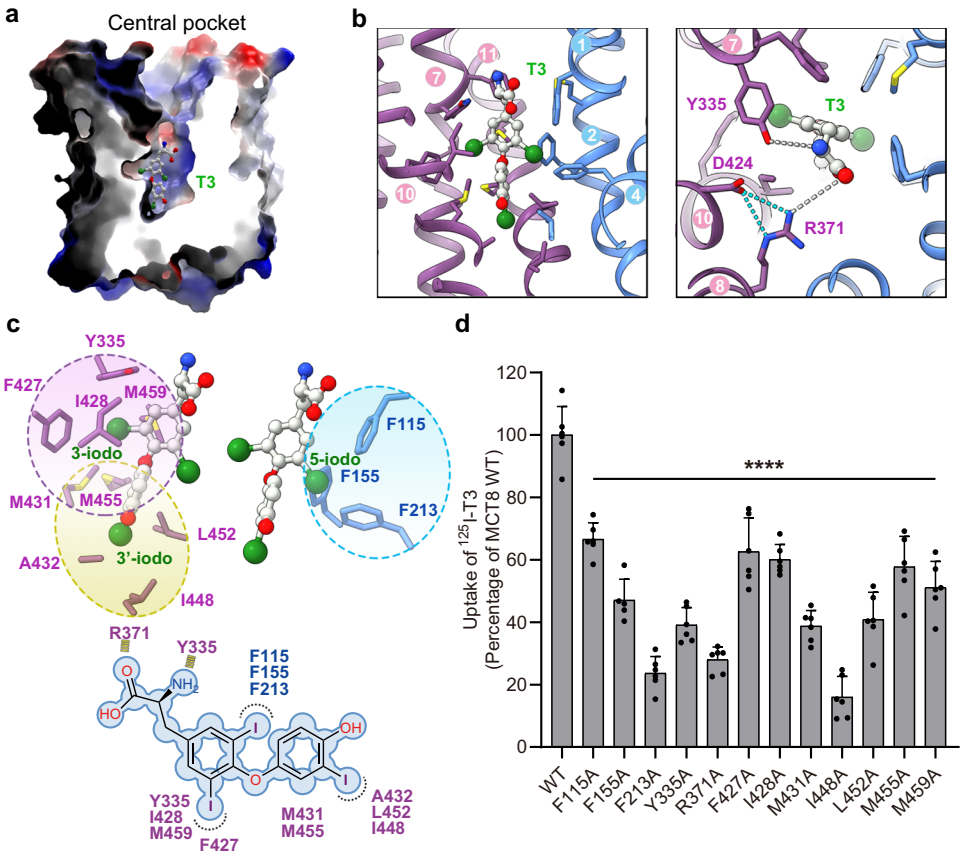

Fig. 3 | T3 recognition and transport by MCT8. a Lateral view of the central pocket. The electrostatic surface potential was computed by ChimeraX. **b** Interactions between MCT8 and T3. *Left panel*: TM1/2/4/7/10/11 enclose the central pocket. The carbon, oxygen and iodine atoms of T3 are colored by gray, red, and green, respectively. *Right panel*: hydrophilic interactions. Hydrogen bonds are marked with white and cyan dashed lines. **c** Iodine-specific interactions between MCT8 and T3. *Upper panel*: The interfaces for 3-, 3′-, and 5-iodo atoms are highlighted in pink, yellow, and blue, respectively. *Lower panel*:A schematic representation of T3 coordination. Hydrophobic interactions are shown as black dashed curves, and hydrophilic interactions are indicated by yellow dashed lines. **d** Biochemical validation of substrate binding residues using a T3 uptake assay. Uptake values were corrected with background T3 uptake levels observed in Hela cells transfected with pCAG empty vector (EV). Six biological repeats were carried out in the experiment (mean ± SEM; $n = 6$). ****$P < 0.0001$ (Student's t test).

central substrate-binding pocket, which is enclosed by TM1/2/4/7/10/11 (Fig. 3a, b).

The carboxyl group of T3 is recognized by Arg371 in TM8 via a charge-charge interaction, a binding mode similar to that observed in MCT1[9] (Fig. 3b, right panel). Mutations in Arg371 of MCT8 result in a complete loss of transport function and are linked to MCT8 deficiency or AHDS[27,28], highlighting the critical role of this residue. The amino group of T3 faces the extracellular side and is potentially stabilized by Tyr335 (Fig. 3b, right panel). The three iodine atoms of T3 fit snugly into distinct hydrophobic cavities. Given the chemical equivalence of the 3- and 3′-iodine atoms in T3, either atom can occupy the same position without chemical distinction between them. The 3-iodine atom resides in a cavity formed by Tyr335, Phe427, Ile428, Met431, Met455, and Met459 (3-iodine cavity); the 3′-iodine atom is positioned near Met431, Ala432, Leu452, Ile448, and Met455 (3′-iodine cavity); and the 5-iodine atom is stabilized by three phenylalanine residues: Phe115, Phe155, and Phe213 (5-iodine cavity). The spatial arrangement of these iodine cavities likely underpins the specific recognition of T3 by MCT8. To validate our structural findings, we generated human MCT8 variants, each containing a single point substitution of the substrate interacting residues, and assessed their T3 transport activities using a cell-based uptake assay. As expected, all mutations led to varying degrees of reduced T3 uptake (Fig. 3d), confirming the functional importance of these interactions.

In previously constructed MCT8 models, residues Arg371, Phe115, Phe213, and Phe427 was also identified as critical for T3 recognition. Biochemical experiments involving point mutations showed similar reductions in transport activity, consistent with our findings[29,30]. However, in those earlier models, residues His118, Met153, Gly208, and His341, which were considered significant for T3 recognition, are located at a considerable distance from T3 in our outward-facing structure. Notably, point mutations of His118, Met153, and Gly208 have been associated with MCT8 deficiencies in patients (Supplementary Table 2), suggesting they may modulate substrate transport through alternative mechanisms (Supplementary Fig. 10).

Inhibition of MCT8 by silychristin

Silychristin, a flavonolignan compound derived from the milk thistle, is a high-affinity inhibitor of MCT8[24]. It consists of three distinct rings: a phenyl ring, a dihydrobenzofuran ring, and a dihydrochromenone ring (Fig. 4a–c).

The dihydrochromenone ring of silychristin is located within the central substrate-binding pocket. Its hydroxyl or carbonyl groups are recognized by Arg371, Ser239, and Asn111. Hydrophobic interactions with this ring are mediated by residues such as Phe115 and Ile428 (Fig. 4a, c). Regarding the dihydrobenzofuran ring, its methylol group forms a hydrogen bond with Asn119, and its carbon portion hydrophobically interacts with a GDN molecule and surrounding residues, including Met151. As for the phenyl ring, its carbonyl group is recognized by the carbonyl group of Met459 (Fig. 4b, c).

https://doi.org/10.1038/s41467-025-58131-8

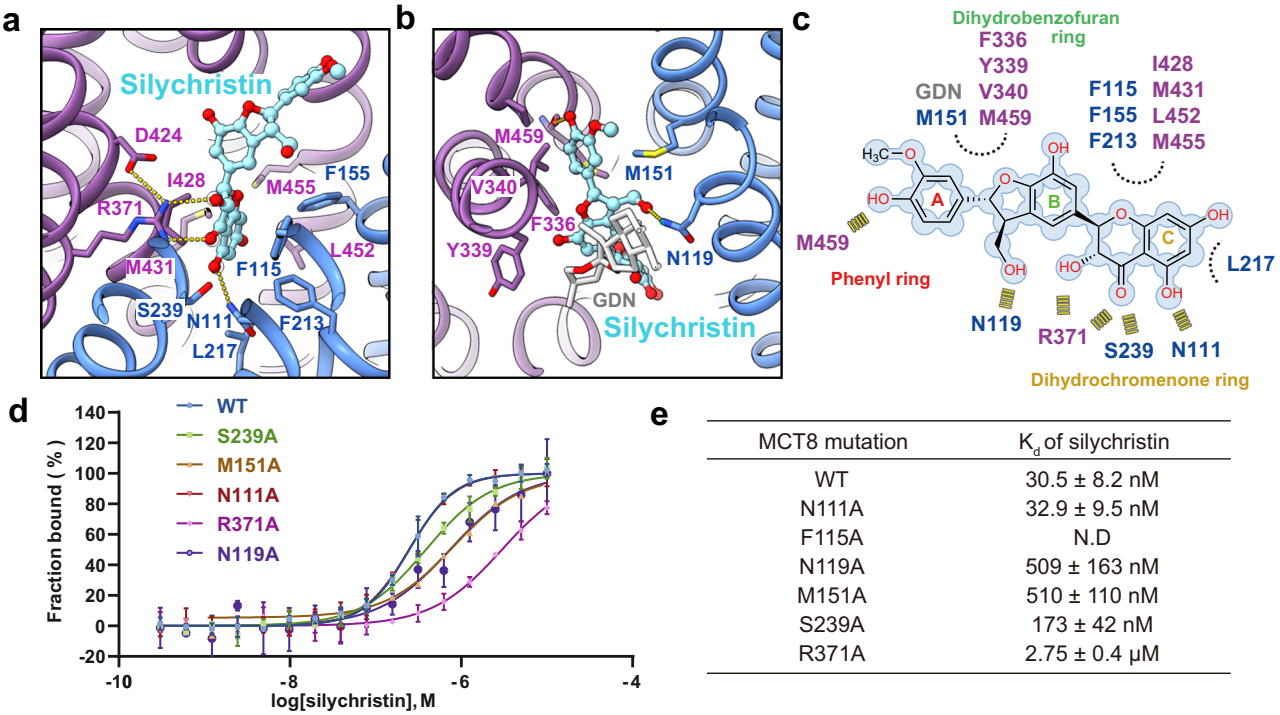

MCT8 mutation	K_d of silychristin
WT	30.5 ± 8.2 nM
N111A	32.9 ± 9.5 nM
F115A	N.D
N119A	509 ± 163 nM
M151A	510 ± 110 nM
S239A	173 ± 42 nM
R371A	2.75 ± 0.4 μM

Fig. 4 | Inhibition of MCT8 by silychristin. a, **b** Interactions between MCT8 and silychristin. Key residues are shown as sticks. The yellow dashed lines indicate hydrogen bonds. **c** A schematic presentation of silychristin coordination by MCT8. **d**, **e** MST measurement of the binding affinities between MCT8 variants and silychristin. Fractions bound of MCT8 variants were normalized against those of WT protein. Three biological repeats were carried out in the experiment (mean ± SEM; n = 3; N.D: not detectable).

To corroborate these structural insights, we employed microscale thermophoresis (MST) to assess the binding affinity between silychristin and various MCT8 variants (Fig. 4d-e). Silychristin exhibited a binding affinity for WT MCT8 with a K_d value of ~31 nM, consistent with previous studies[24]. The F115A mutation resulted in a complete loss of detectable binding between silychristin and MCT8. Variants N119A, M151A, S239A, and R371A showed significantly reduced binding affinity, with decreases ranging from approximately eight- to one-hundred-fold. N111A mutation had no substantial effect on binding affinity. These results are generally in line with our structural observations.

Discussion

Many transporters can perform their functions in both monomeric and dimeric forms, yet the precise mechanisms underlying this phenomenon remain unclear. In this study, we reveal the intricate dimerization interface of MCT8, mediated by TM3 and TM6 within the NTD, along with a phospholipid. This dimerization manner is distinct from other members of the MCT family. For example, MCT1 forms a heterodimer with the transmembrane glycoprotein Basigin (or CD147), while MCT2 dimerizes through interactions between TM1/5 in the NTD and TM6/8 in the CTD (Supplementary Fig. 7a, b; Supplementary Table 2). Compared to other resolved structures in the MFS, MCT8 shares similarities with NTR1.1[31], as both are dimerized via TM3/6 (Supplementary Fig. 7c; Supplementary Table 2). Moreover, lipids are increasingly recognized for their role in facilitating dimerization or the assembly of membrane protein complexes, as seen in the case of the norepinephrine transporter (NET)[32], where lipids mediate dimer formation (Supplementary Fig. 7d). The presence of a lipid molecule at the dimerization interface of MCT8 provides valuable insights into its dimerization mechanism and may offer clues for understanding similar processes in other transporters.

Prior research has suggested that MCT8 dimerization is essential for its transport function[33]. However, our in vitro transport assays indicate that the substrate transport by MCT8 is not significantly affected by whether it is in a dimeric or monomeric form. One possible explanation for this discrepancy lies in the involvement of a hydrophilic cluster in MCT8 dimerization (Fig. 2c, right panel). In the monomeric state, hydrophilic residues such as His186 in TM3 and Gln264 in TM6 are exposed, which may be suboptimal within the hydrophobic membrane bilayer environment (Fig. 5, left panel). Upon dimerization, these residues become embedded within the interface, fostering a more stable structure within the membrane (Fig. 5, right panel). This effect is analogous to the interaction observed between Asn187 in TM6 of MCT1 and Glu218 in the single TM helix of its chaperone Basigin, where hydrogen bonding between the two residues aids in concealing hydrophilic residue in the membrane[9]. In this context, the formation of an MCT8 homodimer may influence its cellular localization or residence time in the cell membrane, potentially affecting its physiological function.

The recognition and transport of THs by MCT8 have long been of interest. Our results uncover the specific interactions between T3 and MCT8, revealing key resides involved in substrate transport. MCT8 exhibits higher selectivity for T3 and T4 over T2 and rT3, and our structural findings provide a potential rationale for this specificity. The structures reveal three iodine cavities designed to accommodate the 3-, 5-, and 3'-iodine atoms of T3, along with a semi-hydrophilic pocket for the 5'-iodine atom of T4. This arrangement likely explains the lower binding affinity of T4 compared to T3 (Supplementary Fig. 8a). For T2 and rT3, the loss of one hydrophobic interaction with the 3- or 5-iodine atom could reduce their binding affinity. In the case of rT3, similar to T4, the 5'-iodine atom exhibits a suboptimal interaction (Supplementary Fig. 8b). These nuanced variations in interactions likely contribute to MCT8's subtype selectivity towards different THs, offering insights into its preferential transport of T3 and T4 over T2 and rT3.

Numerous mutations linked to MCT8 deficiency in patients have been identified (Supplementary Table 3). In vitro studies using patient-derived induced pluripotent stem cells (iPSCs) demonstrate that

https://doi.org/10.1038/s41467-025-58131-8

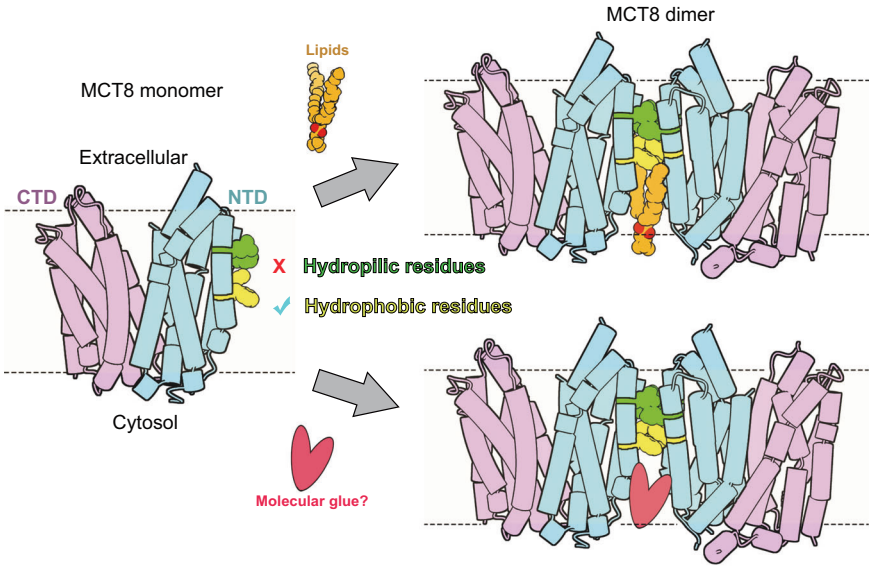

Fig. 5 | Dimer formation of MCT8. Monomeric MCT8 in the membrane. The hydrophilic cluster (highlighted in green), formed by His186, Ser189, Thr268, and Ser267, is not favored within the hydrophobic membrane environment. Hydrophobic cluster is colored yellow. Dimeric MCT8 in the membrane. Lipid binding promotes MCT8 dimerization, which buries the hydrophilic cluster. Lipid-like compounds (highlighted in red) have the potential to act as molecular glues, facilitating MCT8 dimer formation.

MCT8 deficiency impairs T3 transport across the BBB, leading to delayed neuronal maturation[34]. The severity of MCT8-deficient phenotypes correlates with the residual T3 transport capacity of each mutant[35,36]. Mapping these single-point mutations onto our obtained structure can help elucidate their effects (Supplementary Fig. 9a). For example, Arg371, contributing to the recognition of the carboxyl group of T3, its mutations to Serine or Cystein may lead to a complete loss of transport function[27,28] (Supplementary Fig. 9b). To further interpret the effects of these mutations, we also used AlphaFold3[37] to predict the structures of these disease-related mutations (Supplementary Fig. 10). Substitution of Met153 in TM2, which typically facing the membrane lipids, with Arg may destabilize MCT8 within the membrane. Mutations such as V161M, G202R/E, and G208D/C could introduce steric clashes with surrounding residues, while R197S/H might disrupt the local hydrogen bond network. Additionally, the capacity of MCT8 to form dimers or oligomers has been considered important for some mutations found in patients with MCT8 deficiency[38]. Further research is needed to gain a comprehensive understanding of how each mutation disrupts transport function and affects protein stability and interactions.

Our structure also reveals the binding pockets of silychristin, raising concerns about its clinical use as a common treatment for liver disease. Given silychristin's high-affinity inhibition of MCT8, its effects on the TH axis in clinical settings warrant careful evaluation. While inhibiting MCT8 may not be a viable treatment for MCT8 deficiency, it can offer a structural basis for screening chemical inhibitors targeting the thyroid axis for other TH-related diseases, such as hypo- or hyperthyroidism. To deal with MCT8 deficiency, efforts to enhance transport activities are essential. The presence of lipid at the dimer interface opens up the possibility of designing lipid-like compounds that could act as molecular glues to promote the dimer formation (Fig. 5, right panel). This strategy could potentially enhance the membrane localization of MCT8 on the blood-brain barrier (BBB) cell membrane, thereby improving its function.

In conclusion, our study resolved two structures of the MCT8 dimer in substrate-bound and inhibitor-bound states. These structural revelations, combined with biochemical assays, deepen our understanding of THs transport and provide a foundation for future research aimed at developing targeted therapeutic strategies for TH-related disorders.

Methods

Cell culture

The *Escherichia coli* strain DH5α was cultured in LB medium (Sigma) at 37 °C and used to generate and amplify plasmids for MCT8 and the mutants. The mammalian HEK293F cells (Invitrogen) were cultured in SMM 293-TII medium (Sino Biological) at 37 °C under 5% CO_2 and were used to express protein.

Protein expression and purification

Human MCT8 cDNA (UniProt ID: P36021) was cloned into a pCAG vector with a C-terminal FLAG tag. All MCT8 mutants were generated with a standard PCR-based strategy. Overexpression of MCT8 WT and mutants was carried out in mammalian HEK293F cells. 2 mg plasmids and 4 mg polyethylenimine (Polysciences) were preincubated in 50 ml fresh SMM 293-TII medium for 15 min before adding into one liter HEK293F cells at a cell density of 2.0×10^6 cells per ml. After 48 h infection, HEK293F cells were harvested and resuspended in the buffer containing 20 mM Tris-HCl pH 8.0, 150 mM NaCl, and then frozen in liquid nitrogen and stored at −80 °C.

For protein purification, cell pellet was thawed on ice and cell membrane was solubilized in lysis buffer containing protease inhibitors (5 μg/ml aprotinin, 1 μg/ml pepstatin, and 5 μg/ml leupeptin; Amresco) and 2% (w/v) n-dodecyl-β-D-maltopyranoside (DDM, Anatrace) at 4 °C for 2 h. The cell membrane debris was precipitated by high-speed centrifugation (18,700 × *g*) at 4 °C for 1 h, and the supernatant was flowed through anti-flag M2 resin (Sigma) at 4 °C. The resin was washed with a buffer containing 20 mM Tris-HCl pH 8.0, 150 mM NaCl, and 0.02% (w/v) glyco-diosgenin (GDN, Anatrace), the protein was eluted with wash buffer plus 0.4 mg/ml FLAG peptide. The elution was concentrated and injected into size-exclusion chromatography (Superose 6 Increase 10/300 GL column; GE Healthcare) with a buffer containing 20 mM Tris-HCl pH 8.0, 150 mM NaCl, and 0.02% (w/v) GDN. The peak fractions were pooled and concentrated for Cryo-EM analysis.

Thyroid hormone uptake experiments

For TH uptake studies, Hela cells (Invitrogen) were seeded at 37 °C under 5% CO_2 in 24-well plates. Cells were transfected at 70% confluency with indicated amount of pCAG (EV) control, or indicated

amount of WT or mutant MCT8 and human μ-crystallin (CRYM), as previously described[21,39]. Two days after transfection, cells were washed with incubation buffer (Dulbecco's phosphate-buffered saline containing 0.1% D-glucose and 0.1% bovine serum albumin) and subsequently incubated for 30 minutes at 37 °C in incubation buffer containing 1 nM unlabeled T3 and 0.02 μCi (97.3 Ci/mmol) [^{125}I] T3(PerkinElmer). After incubation, cells were briefly rinsed with the incubation buffer and lysed using 2% (w/v) Triton X-100. Radioactivity in the lysates was quantified using a gamma counter.

All assays were performed in three biologically independent experiments. For each biological experiment, we performed 2 technical replicates. To calculate values relative to 100%, we normalized the data by dividing the measurements obtained from mutant proteins by those obtained from the wild-type (WT) protein. Non-specific binding was determined by utilizing pCAG (EV), which served as a control to remove the cell's endogenous transport.

Microscale thermophoresis (MST) binding assay

MST assays was performed using a Monolith NT Label-free system (manufactured by NanoTemper Technologies GmbH), setting the LED power at 20% and MST power at 60%. The proteins under investigation, including MCT8 WT and its variants, were diluted in an MST-specific buffer. This buffer comprised 20 mM Tris-HCl (pH 8.0), 150 mM NaCl, and 0.02% (w/v) GDN. To assess inhibition, a range of inhibitor concentrations were prepared in a serial dilution and then mixed with the MCT8 protein samples.

Cryo-EM sample preparation and data acquisition

The purified MCT8 was concentrated to approximately 10 mg/mL and separately incubated with 1.5 mM T3 and 4 mM silychristin for 30 min before being applied to the grids. The substrate and inhibitor were purchased from MedChemExpress. Aliquots (4 μl) of the protein complex were placed on glow-discharged holey carbon grids (Quantifoil Au R1.2/1.3, 300 mesh). The grids were blotted for 3.0 s and flash-frozen in liquid ethane cooled by liquid nitrogen with Vitrobot (Mark IV, Thermo Fisher Scientific). For the MCT8-Silychristin complex, electron micrographs were acquired on a Titan Krios electron microscope (Thermo Fisher) operating at 300 kV, equipped with a Gatan K3 Summit detector, a Cs corrector, and a GIF Quantum energy filter (slit width 20 eV). Movie stacks were automatically collected using AutoEMation[40], with the energy filter set to a slit width of 20 eV and a preset defocus range from −2.0 μm to −1.5 μm, in super-resolution mode at a nominal magnification of 64,000. For the MCT8-T3 complex, electron micrographs were acquired on a Titan Krios electron microscope (Thermo Fisher) operating at 300 kV and equipped with a Gatan K3 Summit detector and a GIF Quantum energy filter. Movie stacks were automatically collected using AutoEMation, with the energy filter set to a slit width of 20 eV and a preset defocus range from −2.0 μm to −1.5 μm, in super-resolution mode at a nominal magnification of 81,000. Each stack consisted of 32 frames recorded over a total exposure time of 2.56 s, with an exposure time of 0.08 s per frame. The total dose was approximately 50 e − /Å^2 for each stack. All 32 frames in each stack were aligned and summed using the whole-image motion correction program MotionCor2[41]. The resulting images were binned to a pixel size of 1.0979 Å for the MCT8-Silychristin complex and 1.0825 Å for the MCT8-T3 complex.

Data processing and model building

Dose-weighted micrographs were used for CTF estimation using patch-CTF in cryoSPARC[25]. Micrographs CTF fit resolution worse than 4 Å were excluded during manual curation. Initial particles were picked from few micrographs using blob picker. Another round of particle picking was done by template picker using 2D templates generated from blob picked particles. Particles were extracted using a box size of 256 pixels and cropped into 128 pixels to speed up early calculation steps. For the T3 dataset, 2,626,300 particles were extracted from 1,733 micrographs. Initial reference was generated using good particles from the T3 dataset. After rounds of 3D classification and removal of redundant particles presenting top views, 130,122 particles were selected for non-uniform and local refinement with C2 symmetry, resulting in a 3.13 Å map. For the silychristin dataset, 2,405,958 particles were picked from 3,623 micrographs. After rounds of 3D classification and removal of redundant particles presenting top views, 276,909 particles were selected for non-uniform and local refinement with C2 symmetry, resulting in a 3.06 Å map.

The initial MCT8 structure was modeled using AlphaFold[42] and fitted into the cryo-EM map with UCSF ChimeraX[43]. COOT[44] was employed for manual adjustments and rebuilding. Ligand restraint files were generated by phenix.elbow, and the models were refined using PHENIX in real space[45,46]. The structures were validated by Clash scores, Molprobity scores, and Ramachandran plot statistics using PHENIX (Supplementary Table 1).

Reporting summary

Further information on research design is available in the Nature Portfolio Reporting Summary linked to this article.

Data availability

Atomic coordinates of MCT8 in the presence of silychristin or T3 have been deposited in the Protein Data Bank (PDB) under the accession codes 8ZKN and 8ZKO. The corresponding electron microscopy maps have been deposited in the Electron Microscopy Data Bank (EMDB), under the accession codes EMD-60200 and EMD-60201. Previously published structures discussed in this work are as follows: 4OH3, 7DUW, 8JZS, 8WX2 and 7BP3. The source data underlying Figs. 2d-e, 3d, 4e and Supplementary Fig 2b are provided as a Source Data file. Source data are provided with this paper.

References

1. Cheng, S. Y., Leonard, J. L. & Davis, P. J. Molecular aspects of thyroid hormone actions. *Endocr. Rev.* **31**, 139–170 (2010).
2. Yen, P. M. & Yen, P. M. Physiological and molecular basis of thyroid hormone action. *Physiol. Rev.* **81**, 1097–1142 (2001).
3. Friesema, E. C., Jansen, J., Milici, C. & Visser, T. J. Thyroid hormone transporters. *Vitam Horm* **70**, 137–167 (2005).
4. Friesema, E. C. et al. Identification of monocarboxylate transporter 8 as a specific thyroid hormone transporter. *J. Biol. Chem.* **278**, 40128–40135 (2003).
5. Van Geest, F. S., Gunhanlar, N., Groeneweg, S. & Visser, W. E. Monocarboxylate transporter 8 deficiency: from pathophysiological understanding to therapy development. *Front. Endocrinol.* **12**, 723750 (2021).
6. Halestrap, A. P. The monocarboxylate transporter family—structure and functional characterization. *IUBMB life* **64**, 1–9 (2012).
7. Halestrap, A. P. The SLC16 gene family–structure, role and regulation in health and disease. *Mol. Asp. Med.* **34**, 337–349 (2013).
8. Johannes, J. et al. Few amino acid exchanges expand the substrate spectrum of monocarboxylate transporter 10. *Mol. Endocrinol.* **30**, 796–808 (2016).
9. Wang, N. et al. Structural basis of human monocarboxylate transporter 1 inhibition by anti-cancer drug candidates. *Cell* **184**, 370–383.e313 (2021).
10. Zhang, B. et al. Cooperative transport mechanism of human monocarboxylate transporter 2. *Nat. Commun.* **11**, 2429 (2020).
11. Dumitrescu, A. M., Liao, X.-H., Best, T. B., Brockmann, K. & Refetoff, S. A novel syndrome combining thyroid and neurological abnormalities is associated with mutations in a monocarboxylate transporter gene. *Am. J. Hum. Genet.* **74**, 168–175 (2004).

12. Friesema, E. C. et al. Association between mutations in a thyroid hormone transporter and severe X-linked psychomotor retardation. *Lancet* **364**, 1435–1437 (2004).
13. Wirth, E. K. et al. Neuronal 3',3,5-triiodothyronine (T3) uptake and behavioral phenotype of mice deficient in Mct8, the neuronal T3 transporter mutated in Allan-Herndon-Dudley syndrome. *J. Neurosci.* **29**, 9439–9449 (2009).
14. Mayerl, S. et al. Transporters MCT8 and OATP1C1 maintain murine brain thyroid hormone homeostasis. *J. Clin. Invest* **124**, 1987–1999 (2014).
15. Roberts, L. M. et al. Expression of the thyroid hormone transporters monocarboxylate transporter-8 (SLC16A2) and organic ion transporter-14 (SLCO1C1) at the blood-brain barrier. *Endocrinology* **149**, 6251–6261 (2008).
16. Dong, H. & Wade, M. G. Application of a nonradioactive assay for high throughput screening for inhibition of thyroid hormone uptake via the transmembrane transporter MCT8. *Toxicol. Vitr.* **40**, 234–242 (2017).
17. Oppenheimer, J. H. Evolving concepts of thyroid hormone action. *Biochimie* **81**, 539–543 (1999).
18. Abdalla, S. M. & Bianco, A. C. Defending plasma T3 is a biological priority. *Clin. Endocrinol. (Oxf.)* **81**, 633–641 (2014).
19. Peeters, R. P. & Visser, T. J. Metabolism of thyroid hormone. *Thyroid Disease Manager (ed. DeGroot, L. J.) [online]* (2015).
20. Gereben, B. et al. Cellular and molecular basis of deiodinase-regulated thyroid hormone signaling. *Endocr. Rev.* **29**, 898–938 (2008).
21. Friesema, E. C., Kuiper, G. G., Jansen, J., Visser, T. J. & Kester, M. H. Thyroid hormone transport by the human monocarboxylate transporter 8 and its rate-limiting role in intracellular metabolism. *Mol. Endocrinol.* **20**, 2761–2772 (2006).
22. Visser, W. E. et al. Evidence for a homodimeric structure of human monocarboxylate transporter 8. *Endocrinology* **150**, 5163–5170 (2009).
23. Federico, A., Dallio, M. & Loguercio, C. Silymarin/silybin and chronic liver disease: a marriage of many years. *Molecules* **22**, 191 (2017).
24. Johannes, J. et al. Silychristin, a flavonolignan derived from the milk thistle, is a potent inhibitor of the thyroid hormone transporter MCT8. *Endocrinology* **157**, 1694–1701 (2016).
25. Punjani, A., Rubinstein, J. L., Fleet, D. J. & Brubaker, M. A. cryoSPARC: Algorithms for rapid unsupervised cryo-EM structure determination. *Nat. methods* **14**, 290–296 (2017).
26. Song, D., Jiao, H. & Liu, Z. Phospholipid translocation captured in a bifunctional membrane protein MprF. *Nat. Commun.* **12**, 2927 (2021).
27. Ono, E. et al. Three novel mutations of the MCT8 (SLC16A2) gene: individual and temporal variations of endocrinological and radiological features. *Clin. Pediatr. Endocrinol.* **25**, 23–35 (2016).
28. Capri, Y. et al. Relevance of different cellular models in determining the effects of mutations on SLC 16 A 2/MCT 8 thyroid hormone transporter function and genotype–phenotype correlation. *Hum. Mutat.* **34**, 1018–1025 (2013).
29. Groeneweg, S. et al. Outward-open model of thyroid hormone transporter monocarboxylate transporter 8 provides novel structural and functional insights. *Endocrinology* **158**, 3292–3306 (2017).
30. Protze, J. et al. Membrane-traversing mechanism of thyroid hormone transport by monocarboxylate transporter 8. *Cell Mol. Life Sci.* **74**, 2299–2318 (2017).
31. Sun, J. et al. Crystal structure of the plant dual-affinity nitrate transporter NRT1. 1. *Nature* **507**, 73–77 (2014).
32. Zhang, H. et al. Dimerization and antidepressant recognition at noradrenaline transporter. *Nature* **630**, 247–254 (2024).
33. Fischer, J. et al. Modulation of monocarboxylate transporter 8 oligomerization by specific pathogenic mutations. *J. Mol. Endocrinol.* **54**, 39–50 (2015).
34. Vatine, G. D. et al. Modeling psychomotor retardation using iPSCs from MCT8-deficient patients indicates a prominent role for the blood-brain barrier. *cell stem cell* **20**, 831–843.e835 (2017).
35. Kinne, A. et al. Surface translocation and tri-iodothyronine uptake of mutant MCT8 proteins are cell type-dependent. *J. Mol. Endocrinol.* **43**, 263–271 (2009).
36. Kinne, A. et al. Essential molecular determinants for thyroid hormone transport and first structural implications for monocarboxylate transporter 8. *J. Biol. Chem.* **285**, 28054–28063 (2010).
37. Abramson, J. et al. Accurate structure prediction of biomolecular interactions with AlphaFold 3. *Nature* **630**, 493–500 (2024).
38. Groeneweg, S. et al. Insights into the mechanism of MCT8 oligomerization. *J. Endocr. Soc.* **4**, bvaa080 (2020).
39. Friesema, E. C. et al. Effective cellular uptake and efflux of thyroid hormone by human monocarboxylate transporter 10. *Mol. Endocrinol.* **22**, 1357–1369 (2008).
40. Lei, J. & Frank, J. Automated acquisition of cryo-electron micrographs for single particle reconstruction on an FEI Tecnai electron microscope. *J. Struct. Biol.* **150**, 69–80 (2005).
41. Zheng, S. Q. et al. MotionCor2: anisotropic correction of beam-induced motion for improved cryo-electron microscopy. *Nat. methods* **14**, 331–332 (2017).
42. Jumper, J. et al. Highly accurate protein structure prediction with AlphaFold. *Nature* **596**, 583–589 (2021).
43. Pettersen, E. F. et al. UCSF ChimeraX: Structure visualization for researchers, educators, and developers. *Protein Sci.* **30**, 70–82 (2021).
44. Emsley, P. & Cowtan, K. Coot: model-building tools for molecular graphics. *Acta Crystallogr. Sect. D: Biol. Crystallogr.* **60**, 2126–2132 (2004).
45. Afonine, P. V. et al. Real-space refinement in PHENIX for cryo-EM and crystallography. *Acta Crystallogr. Sect. D: Struct. Biol.* **74**, 531–544 (2018).
46. Liebschner, D. et al. Macromolecular structure determination using X-rays, neutrons and electrons: recent developments in Phenix. *Acta Crystallogr. Sect. D: Struct. Biol.* **75**, 861–877 (2019).

Acknowledgements

We thank F. Yang and X. Li for technical support during EM data collection. We thank the Tsinghua University Branch of China National Center for Protein Sciences (Beijing) for providing the cryo-EM facility support and the computational facility support. This work was funded by the National Natural Science Foundation of China (32171204, C.Y.), Beijing Nova Program (Z201100006820039), the National Key R&D Program of China (2020YFA0509301, C.Y.), Beijing Frontier Research Center for Biological Structure, State Key Laboratory of Membrane Biology, Tsinghua University Initiative Scientific Research Program (20221080032, 20231080037, C.Y.), and Start-up funds from Tsinghua-Peking Center for Life Sciences and Tsinghua University.

Author contributions

C.Y. conceived the project. J.T. and C.Y. designed all experiments. J.T., Y.X. and J.Q. performed the experiments. F.K., C.Y. and A.Z. contributed to the data processing and structure determination. C.Y., T.J., F.K. and Y.X. contributes to structural analysis. All authors contributed to manuscript preparation. J.T. and C.Y. wrote the manuscript.

Competing interests

The authors declare no competing interests.

Additional information

Supplementary information The online version contains supplementary material available at https://doi.org/10.1038/s41467-025-58131-8.

Correspondence and requests for materials should be addressed to Chuangye Yan.

Peer review information *Nature Communications* thanks the anonymous reviewers for their contribution to the peer review of this work. A peer review file is available.